



ARTICLE

Novel-smoothened inhibitors for therapeutic targeting of naïve and drug-resistant hedgehog pathway-driven cancers

Qing-rou Li¹, Hui Zhao¹, Xue-sai Zhang¹, Henk Lang² and Ker Yu¹

The G protein-coupled receptor (GPCR) smoothened (SMO) is a key signaling component of the sonic hedgehog (Hh) pathway and a clinically validated target for cancer treatment. The FDA-approved SMO inhibitors GDC-0449/Vismodegib and LDE225/Sonidegib demonstrated clinical antitumor efficacy. Nevertheless, relatively high percentage of treated patients would eventually develop acquired cross resistance to both drugs. Here, based on published structure and activity of GDC-0449 inhibitor class, we replaced its amide core with benzimidazole which retained bulk of the SMO-targeting activity as measured in our Hh/SMO/Gli1-reporter system. Synthesis and screening of multiple series of benzimidazole derivatives identified HH-1, HH-13, and HH-20 with potent target suppression (IC_{50} : $<0.1 \mu\text{mol/L}$) in the reporter assays. In NIH3T3 cells stimulated with a secreted Hh (SHH), these inhibitors dose dependently reduced mRNA and protein expression of the endogenous pathway components PTCH-1, Gli1, and cyclin D1 resulting in growth inhibition via G_0/G_1 arrest. Mechanistically, the SMO-targeted growth inhibition involved downregulation of mTOR signaling inputs and readouts consistent with diminished mTORC1/mTORC2 functions and apoptosis. In mice, as with GDC-0449, orally administered HH inhibitors blocked paracrine activation of stromal Hh pathway in Calu-6 tumor microenvironment and attenuated growth of PTCH^{+/-}/P53^{-/-} medulloblastoma allograft tumors. Furthermore, HH-13 and HH-20 potently targeted the drug-resistant smoothened SMO-D473H (IC_{50} : $<0.2 \mu\text{mol/L}$) compared to the poor inhibition by GDC-0449 (IC_{50} : $>60 \mu\text{mol/L}$). These results identify HH-13 and HH-20 as potent inhibitors capable of targeting naïve and drug-resistant Hh/SMO-driven cancers. The current leads may be optimized to improve pharmaceutical property for potential development of new therapy for treatment of Hh pathway-driven cancers.

Keywords: hedgehog; smoothened inhibitor; paracrine; acquired drug resistance

Acta Pharmacologica Sinica (2019) 40:257–267; <https://doi.org/10.1038/s41401-018-0019-5>

INTRODUCTION

The sonic hedgehog (Hh) signaling pathway is essential for embryonic development and organ formation [1]. Upon completing embryogenesis, the Hh pathway generally goes silent while remains active in certain circumstances such as hair follicle maintenance and tissue repair [2]. The canonical Hh signaling is initiated by the Hh ligand binding to the pathway suppressor PTCH-1. This action rapidly stimulates the key G protein-coupled receptor (GPCR) smoothened (SMO) leading to activation of Gli transcription factors and pathway biological function [3].

Aberrant Hh/SMO/Gli1 signaling pathway is linked to pathogenesis of numerous human cancers including advanced basal-cell carcinoma (BCC), medulloblastoma (MB), and other solid tumors [4, 5]. Studies also identified at least three mechanisms of Hh pathway activation in tumorigenesis, including the autocrine ligand-dependent, paracrine ligand-dependent, [6] and ligand-independent activation [3, 5, 7]. In the ligand-independent setting, tumors were frequently found to possess the genetic loss of PTCH-1, resulting in constitutive over-activation of SMO [3]. Employing gene depletion technique or small molecule inhibitors, targeting Hh pathway led to antitumor efficacy in preclinical models of BCC and MB both in vitro and in vivo [8]. These earlier findings draw increasing attention to Hh/SMO pathway in cancer biology and therapy development. Thus far, two SMO inhibitors Vismodegib

(GDC-0449) and Sonidegib (LDE225) have received FDA approval for cancer treatment. In clinical trials, GDC-0449 and LDE225 were used as single agent therapy in BCC and MB patients and achieved impressive clinical response in overall disease control [9–11].

Acquired drug resistance is a major and evolving challenge in targeted cancer therapy, including those with the approved SMO inhibitors [12, 13]. Clinical experience indicated that GDC-0449 and LDE225 could confront a cross resistance [14]. To address this issue, resistance mechanisms are under intense investigation. Employing genomic analysis of GDC-0449-resistant tumors, several SMO gene mutations have been discovered [15]. In particular, a recurring mechanism involves the SMO-D473H mutation, which blocks GDC-0449 or LDE225 from efficient binding to the mutant SMO protein. In a study, nearly 40% BCC patients who acquired resistance were shown to contain SMO mutations and 17% patients carry the SMO-D473H molecular type [16]. More recently, new generation SMO inhibitors such as TAK-441, LEQ-506, and IPI-926 have entered clinical studies [17–19]. These latest agents could overcome mutant SMO activity in the preclinical setting and their clinical performances are eagerly awaited.

In this study, we aimed to design and screen a series of new SMO inhibitors. We show that several compounds not only

¹Department of Pharmacology, Fudan University School of Pharmacy, 201203 Shanghai, China and ²Sundia MediTech, 050031 Shijiazhuang, China

Correspondence: Ker Yu (keryu@fudan.edu.cn)

These authors contributed equally: Qing-rou Li, Hui Zhao.

Received: 20 September 2017 Revised: 31 January 2018 Accepted: 11 February 2018

Published online: 18 May 2018

displayed potent suppression of the Hh pathway function but also are able to overcome the drug resistance caused by SMO-D473H.

MATERIALS AND METHODS

Chemicals and cell culture

The current HH series of compounds were synthesized as described [20, 21]. GDC-0449 was purchased from BiochemPartner (Shanghai). Smoothened agonist (SAG) was purchased from Sant Cruz Biotechnology. Inhibitors were dissolved in DMSO as 20 mmol/L stock solution and were freshly diluted before assays. HEK293T, NIH3T3, and Calu-6 cell lines were purchased from American Type Culture Collection (ATCC) and were cultured as recommended.

SMO-D473H mutagenesis

p-CMV6-Smo-D473H point mutation was established with standard site-directed mutagenesis technique. Primers were as follows: F: 5'-TGAAGAAGTGGTAGAAGTGGCAGCTGAAGGTAAT-3'; R: 5'-CACTTCTACCACTTCTTCAACCAGGCTGAGT-3'.

Secreted hedgehog (SHH) condition medium (SHH-CM)

293T cells were plated 3×10^6 cells per well in 55 cm² dish. The next day, cells were transfected with pcDNA3.1 ShhN construct encoding the N-terminus secreted Hh fragment (SHH, Addgene) using Lipofectamine 2000 (Invitrogen). After 24 h, medium was replaced with DMEM containing 2% FBS. The SHH-CM was collected at 48 and 72 h, pooled and then centrifuged at 1000 rpm for 10 min. The supernatant was stored at 4 °C until use within a week.

Gli1-luciferase reporter assay

NIH3T3 cells were plated in 96-well plate at 5×10^3 cells per well for overnight. Cells were transfected with 180 ng $8 \times 3'$ Gli-BS-delta51-LucII (Rikagaku KENkyusho/Institute of Physical and Chemical Research) and 20 ng TK-Renilla using Lipofectamine 2000. After 6 h, medium was refreshed to 10% new-born calf serum (NBCS) in DMEM for 24 h. On the day of inhibitor assay, cells were fed with medium containing 0.5% NBCS for 1 h, then stimulated with 100 ng/mL SAG or 50 μ L SHH-CM without or with various testing inhibitor compounds. Forty-eight hours later, cells were lysed and tested for luciferase activity with Dual-Luciferase Reporter Assay Kit (YPHbio, Beijing). For GDC-0449-resistant assay system, 293T cells were plated in 96-well plate, 5×10^3 per well. The next day, cells were transfected with 100 ng $8 \times 3'$ Gli-BS-delta51-LucII and 100 ng p-CMV6-SMO-WT or p-CMV6-SMO-D473H plasmid DNA for 24 h, treated with various inhibitors for 48 h, followed by luciferase activity assay performed as described above.

RT-PCR assay of gene expression

Cells or tumors were harvested and extracted total RNA according to SuperfecTRI total RNA Isolation Reagent (Pufei, Shanghai). Reverse transcription of mRNA into cDNA was performed with RevertAid First Strand cDNA Synthesis Kit (Fermentas), subjected to PCR with FastStart Universal SYBR Green Master (Rox) Kit (Roche) in iQ5 Cycler (Bio-Rad). PCR primers included mouse Gli1, F: 5'-GCAGTGGGTAACATGAGTGTCT-3', R: 5'-AGGCACTAGAGTTGAGGAATTGT-3'; mouse PTCH-1, F: 5'-CTCTGGAGCAGATTTCAAGG-3', R: 5'-TGCCGAGTTCTTTGAATG-3'; mouse CyclinD1, F: 5'-GTGCGTGCAGAAGGAGATTG-3', R: 5'-AGGTTCAAGCCTTGATC-3'; mouse RPL19, F: 5'-AGAAGGTGACTGGATGAGA-3', R: 5'-TGATACATATGGCGGTCAATCT-3'; human GAPDH, F: 5'-TTCACCACATGGAGAAGGC-3', R: 5'-GGCATGGACTGTGGTCATGA-3'; human SMO, F: 5'-ACCTATGCCTGGCACACTTC-3', R: 5'-GTGAGGACAAAGGGGAGTGA-3'. Relative gene expression was analyzed and normalized to RPL19 (mouse genes) or GAPDH (human genes).

Cell proliferation and cell cycle analysis

Cell proliferation was assayed with the indicated treatments for 3 days using MTS reagent (Promega) as previously described [22]. For cell cycle profiling, cells were treated as indicated for 24 h and analyzed in a Becton Dickinson FACS Calibur flow cytometer by collecting 10,000 events.

Apoptosis assay

293T cells were transiently transfected with p-CMV6-SMO-WT for 24 h, treated with inhibitors for 48 h. The cells were harvested, stained with Annexin V-FITC/PI staining kit (KeyGEN BioTECH, Cat# KGA108) and analyzed by FACS.

Calu-6 human lung tumor xenografts

Animal studies were performed under protocols approved by Institutional Animal Care and Use Committee (IACUC) of Fudan University. Balb/c female nude mice (Shanghai Sippr-BK laboratory animal Co. Ltd.) between 6 and 8 weeks of age were subcutaneously injected 4×10^6 Calu-6 cells in a Matrigel (BD Biosciences) /DMEM mixture. When tumor size reached ~ 400 mm³, mice were treated twice a day (bid) with vehicle (20% HP- β -CD) or 75 mg/kg GDC-0449, HH-1, HH-13, and HH-20 by oral gavage. Mice were killed after five treatments. Tumors were collected and analyzed for mouse stromal cell mRNA level through RT-PCR.

PTCH^{+/-}/P53^{-/-} mouse medulloblastoma (MB) model

C57BL/6J PTCH1tmIMps/J (PTCH^{+/-}) was purchased from Jackson Laboratory, C57BL/6J B6.129S2-Trp53tmTyj/JNju (P53^{-/-}) was purchased from Model Animal Research Center of Nanjing University. PTCH^{+/-}/P53^{-/-} mouse MB model on a C57BL/6 background was generated as previously described [23]. Mice with spontaneous MB tumors were sacrificed. Tumors were dissected from cerebellum and then subcutaneously implanted into Balb/c female nude mice (6–8 week) (P1 tumors). The grafted tumors were allowed to grow to 300–500 mm³ before harvested and serially passaged (P2 and P3 tumors). For efficacy studies, tumor fragments were implanted into flank of female nude mice. Mice bearing staged tumors (150–200 mm³ in size) were randomized into groups ($n = 8$), treated orally with vehicle or the indicated inhibitors via a twice daily (bid) regimen. Tumor growth was monitored with caliper every 2 days. Tumor volume was calculated as V (mm³) = $L \times W \times W/2$. Tumors were collected at the end of study.

Immunoblotting

For standard assay of inhibitor effects on cellular biomarker expression, cells were plated at predetermined density in 6-well culture plates for overnight, treated with SHH-CM without or with inhibitors for the indicated doses and time. Cells were lysed with NuPAGE-LDS lysis buffer (Invitrogen) and immunoblotted with antibodies including Gli1 (Santa Cruz); PTCH-1, cyclin D1, P-TSC2 (T1462), P-mTOR(S2481), mTOR (Cell Signaling Technology); SMO (Abgent); P-AKT(S473), AKT, P-S6(S235/236), S6 (Abcam-Epitomics); MCL-1 (Affinity); β -actin, GAPDH (Bioworld). Immunoblotting of in vivo tumors were performed as described previously [22].

Statistical analysis

All numerical data processing and statistical analysis were performed with Microsoft Excel Software; values were expressed as means \pm SD. *P* values were calculated using unpaired two-tailed Student *t* test.

RESULTS

Discovery of benzimidazole derivatives as novel SMO inhibitors To identify novel SMO inhibitors, we first analyzed the published structure and activity information for GDC-0449 and its analogs.

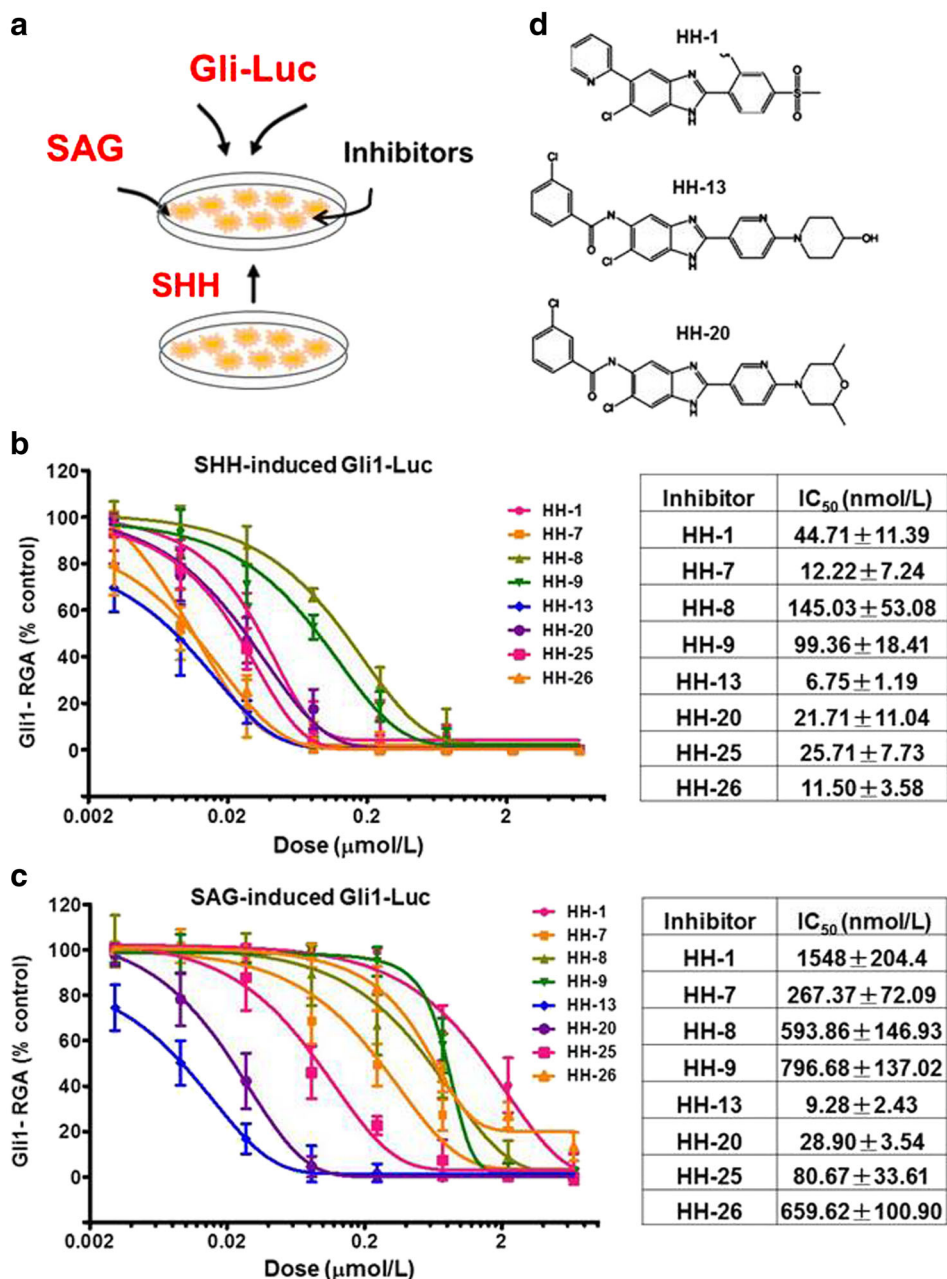


Fig. 1 Screening of newly designed SMO inhibitor compounds in NIH3T3 cell Gli1 report gene assay. **a** Gli1-luciferase assay scheme is shown. The assays were performed as described in Method. **b, c** Dose–response inhibition curves (left) and IC₅₀ values (right) are shown. The cellular Hh pathway activation was induced with SHH-CM (**b**) or SAG (**c**). **d** Chemical structures of HH-1, HH-13, and HH-20 are shown

This analysis led to the design and synthesis of multiple series of substituted benzimidazole derivatives [20, 21]. Antagonists were screened by two versions of cell-based Gli1-reporter assay. The Gli1-luc reporter activity was induced either with a secreted hedgehog-condition medium (SHH-CM) or with a known SMO agonist (SAG) compound (Fig. 1a). In the SHH-induced reporter system, numerous compounds displayed potent antagonist activity with IC₅₀ value range <200 nmol/L (Fig. 1b). When screened in the SAG-induced reporter system, while majority of the compounds showed a significantly reduced potency, compounds HH-13 and HH-20 retained potent antagonist activity (Fig. 1c). Specifically, HH-13 and HH-20 elicited respective IC₅₀ values of 6.8 and 21.7 nmol/L in SHH-CM system, and showed 9.3 and 28.9 nmol/L in SAG system (Fig. 1b, c). Meanwhile, we performed in vivo bioavailability studies and found that the

mouse oral exposure ratio for compound HH-1 was significantly higher than other compounds (Figure S1A). These results and additional findings (see below) led us to select HH-1, HH-13, and HH-20 (Fig. 1d) as hit molecules.

Targeting of the Hh pathway gene transcription

In serum-starved NIH3T3 stimulated with SHH-CM, mRNA expression of the Hh pathway genes Gli1, PTCH-1, and cyclin D1 increased by ~60-fold, 20-fold, and 2-fold, respectively (Fig. 2a). To test the inhibitory effect on these genes, serum-starved NIH3T3 cells were induced with SHH-CM in the presence of inhibitors for 48 h. All three inhibitors dose dependently reduced mRNA levels for Gli1 (Fig. 2b), PTCH-1 (Fig. 2c) with an overall potency order of HH-13 > HH-20 > HH-1. Specifically, both HH-13 and HH-20 inhibited these two genes at doses as low as 0.01–0.05 μmol/L, while

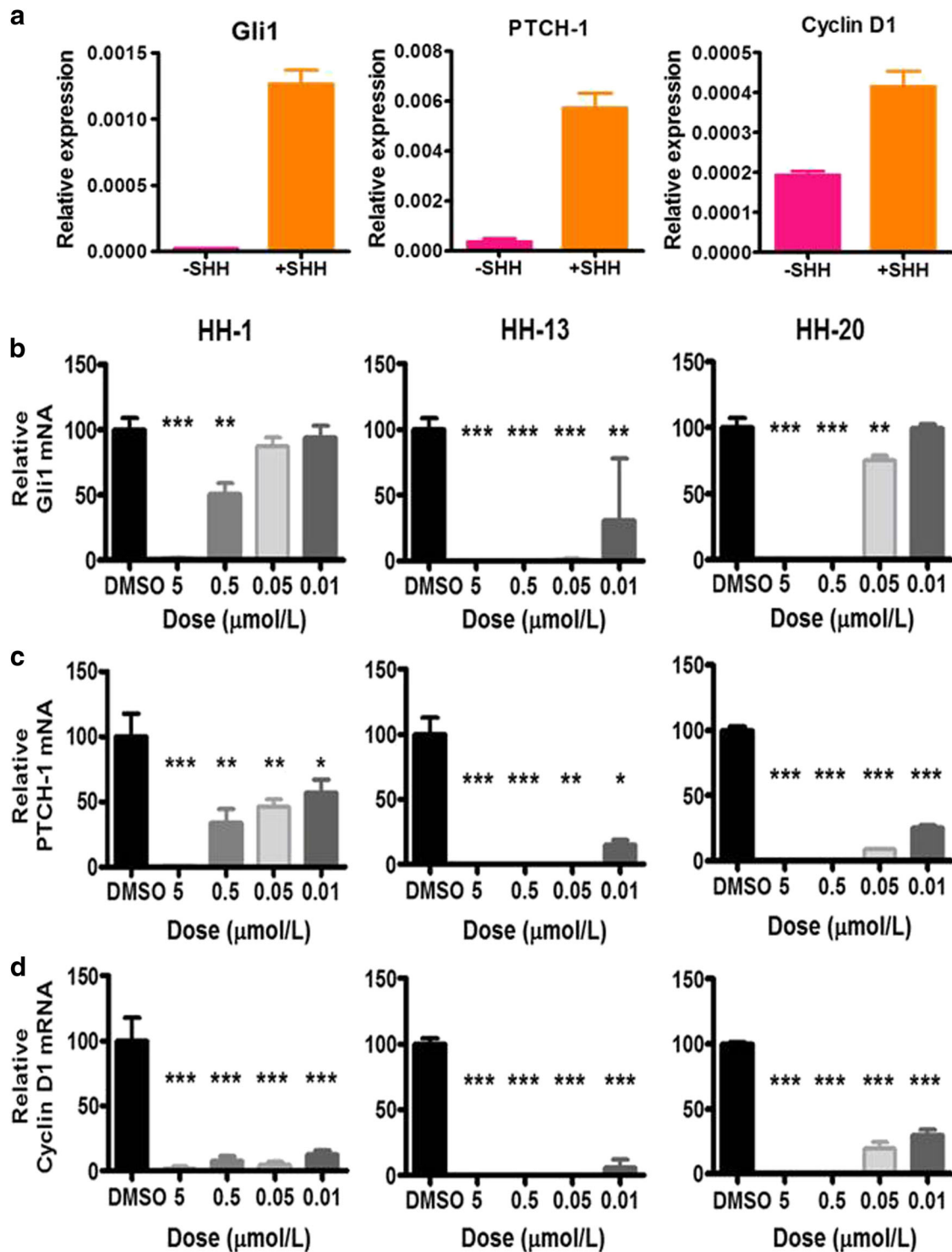


Fig. 2 New SMO inhibitors target the Hh pathway gene expression. **a** mRNA levels of Gli1, PTCH-1, and cyclin D1 were analyzed after serum-starved NIH3T3 cells were induced with SHH-CM for 48 h as described in Methods. **b–d** Serum-starved NIH3T3 cells were similarly induced by SHH-CM with vehicle or the indicated inhibitors for 48 h. Cells were analyzed for mRNA levels of Gli1 (**b**), PTCH-1 (**c**), and cyclin D1 (**d**). Relative expression levels are shown. Statistical analysis (treated vs. DMSO control): * $P < 0.05$; ** $P < 0.01$; *** $P < 0.001$

HH-1 showed inhibition at 0.5 μmol/L (Fig. 2b, c). Interestingly, all three inhibitors profoundly inhibited the expression of cyclin D1 even at 0.01–0.05 μmol/L (Fig. 2d). These results demonstrate a dose-dependent inhibition of the endogenous Hh-target gene transcription in response to treatment with HH-1, HH-13, and HH-20.

Inhibition of Hh ligand-dependent cell growth

We next established an Hh pathway-dependent growth assay system. Treatment of NIH3T3 cells with SHH-CM led to a sharp increase in cell growth which could be suppressed by GDC-0449 (Fig. 3a). In this assay system, while the vast majority of inhibitors displayed an expected inhibitory activity, HH-13 and HH-20

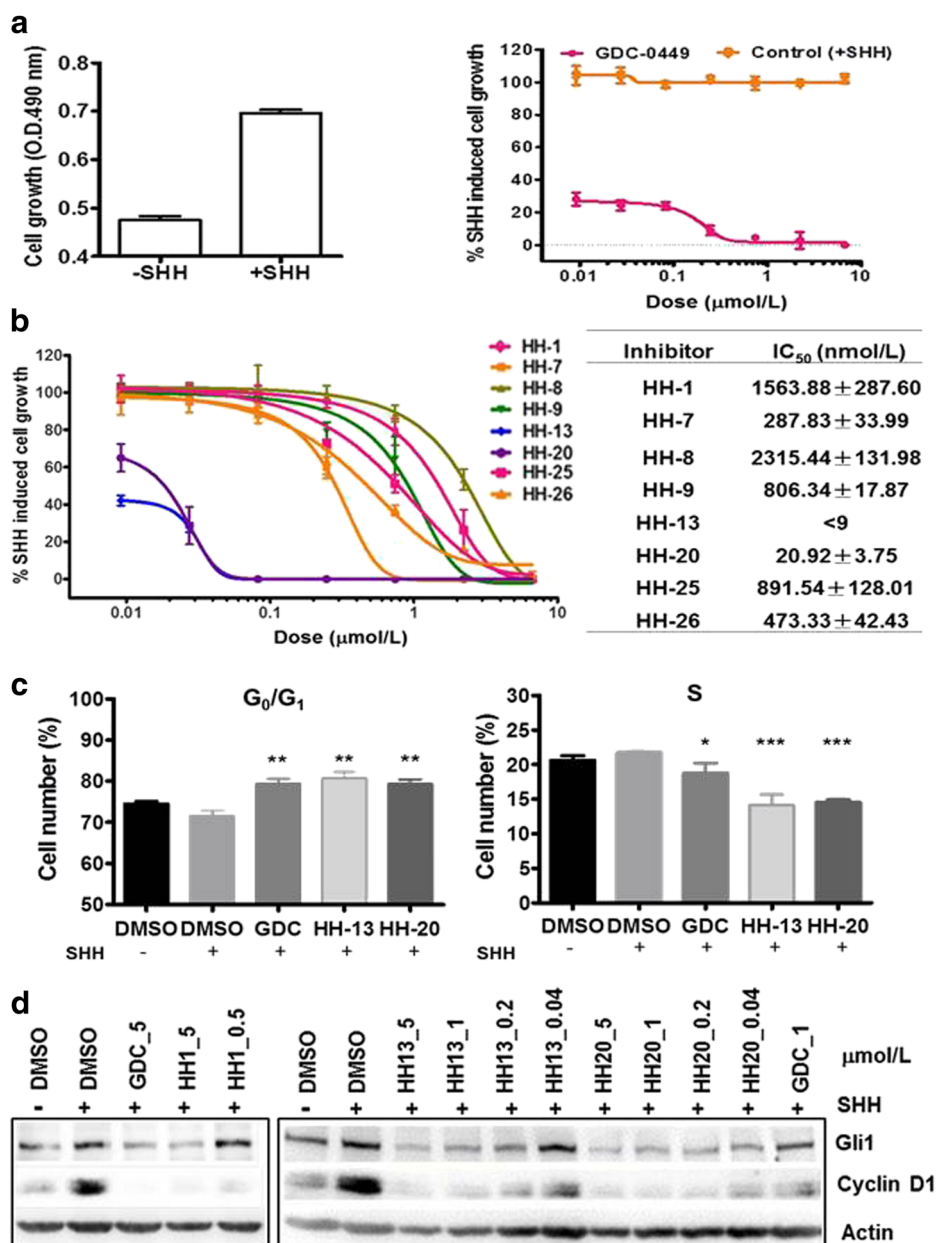


Fig. 3 Targeting of Hh pathway leads to inhibition of cell proliferation. **a** The SHH-induced NIH3T3 cell proliferation model was established (left panel) and validated with GDC-0449 (right panel). Cells were induced by SHH-CM for 72 h and measured for cell proliferation as described in Methods. **b** Cells as in **a** were treated with vehicle or the indicated inhibitors for 72 h followed by proliferation assay using MTS reagent. Growth inhibition dose–response curves are shown (left panel) and IC₅₀ values are shown (right panel). **c** Cells as in **a** were treated with the indicated inhibitors for 24 h, subjected to cell cycle analysis by FACS. Cell populations in G₀/G₁ and S phase are shown. **d** Cells as in **a** were treated with the indicated inhibitors for 48 h. Total cell lysates were collected and subjected to immunoblotting. Statistical analysis (treated vs. DMSO control): **P* < 0.05; ***P* < 0.01; ****P* < 0.001

showed the most potent and consistent suppression of cell growth with IC₅₀ values of <9 nmol/L and 21 nmol/L, respectively (Fig. 3b). Cell cycle analysis revealed a significant increase in the G₀/G₁ phase and decrease in S phase distribution in cells treated with GDC-0449, HH-13, or HH-20 (Fig. 3c). Consistently, immunoblotting of the inhibitor-treated cells demonstrated a downregulation in protein levels of Gli1 and cyclin D1 compared to that of vehicle-treated cells (Fig. 3d). These results suggest that similar to GDC-0449, the current series of HH inhibitors could effectively target the Hh signaling pathway function leading to growth suppression via a blockade in G₀/G₁ cell cycle progression.

Downregulation of mTOR pathway and induction of apoptosis in inhibitor-treated cells
 Intracellular mTOR pathway plays a major role in cell growth and survival. We therefore examined signaling status of mTOR complexes (mTORCs) as the potential downstream mediators of SMO-targeted growth inhibition. We found that the SHH-induced phosphorylation of mTORC1 biomarker P-S6 (S235/236) and mTORC2 biomarker P-AKT (S473) in NIH3T3 cells were potently and profoundly inhibited by HH-13 and HH-20 with effective doses at <1 $\mu\text{mol/L}$ (Fig. 4a). For comparison, 1 $\mu\text{mol/L}$ GDC-0449 near completely suppressed P-S6 and consistently but partially reduced P-AKT. These results indicated that the anti-proliferative

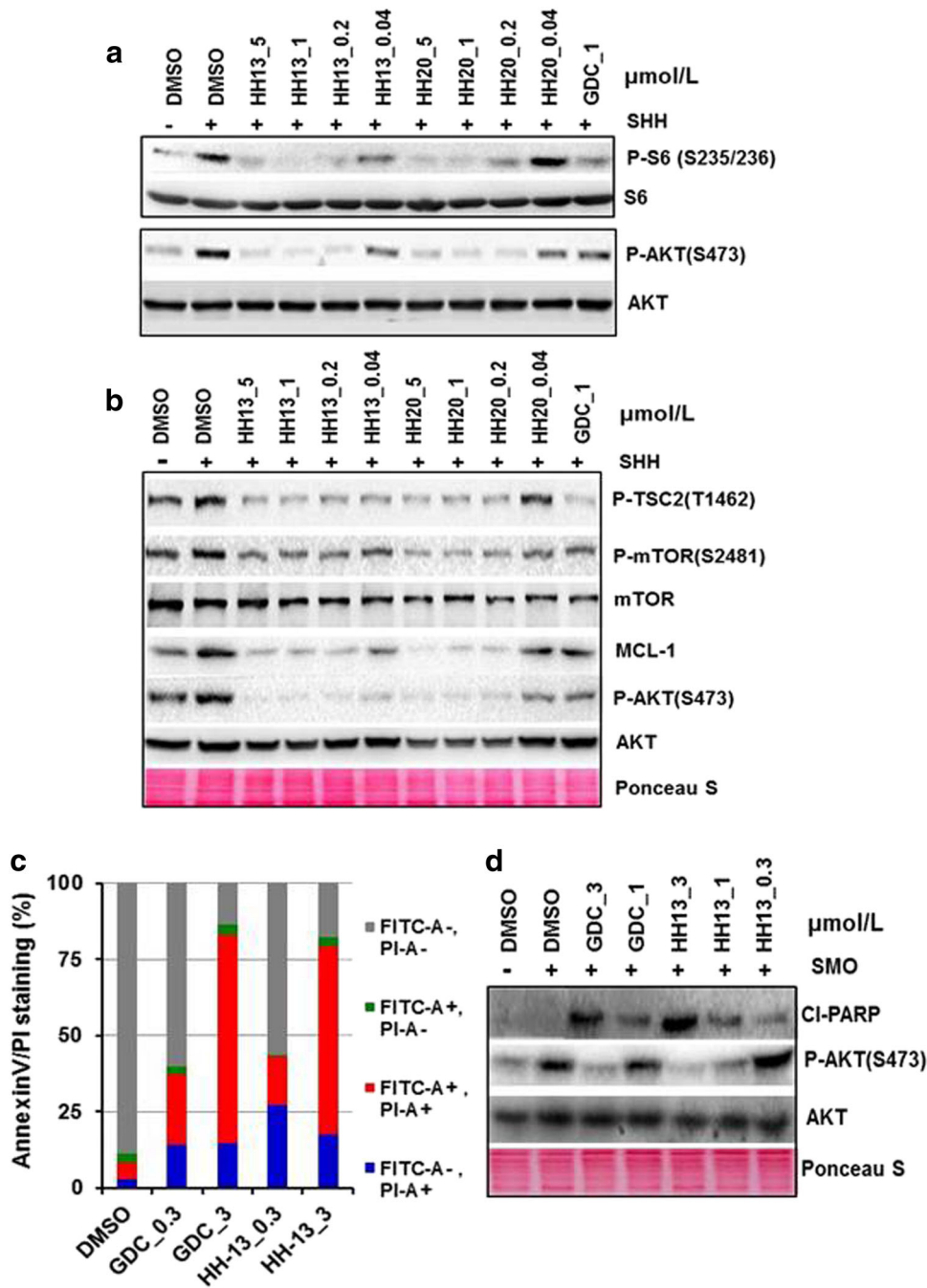


Fig. 4 Targeting of Hh pathway function leads to downregulation of mTOR/AKT activity. **a, b** Serum-starved NIH3T3 cells were induced with SHH for 48 h without or with the indicated inhibitors. Total cell lysates were prepared and subjected to immunoblotting as indicated. **c** 293T cells were transfected with SMO-WT expression vector for 24 h, treated with inhibitors for 48 h, subjected to Annexin V-FITC/PI staining. Positive populations as analyzed by FACS are plotted. **d** Cells as in **c** were collected and immunoblotted

effects of the current SMO inhibitors are mediated through downregulation of mTOR activity. We examined additional mTOR readouts and signaling regulation. In cells treated with HH-13, HH-20, and GDC-0449, there were substantial reduction in P-TSC2 (T1462) as well as partial loss of P-mTOR (S2481) and mTOR, all of which are consistent with a diminished signaling input to mTOR network (Fig. 4b). Importantly, targeting of SMO in this setting also dramatically downregulated level of MCL-1, an apoptosis inhibitory protein recently shown to be protected by mTORC2/AKT axis [24] (Fig. 4b). We then analyzed 293T human cells transfected with the wild-type smoothened (SMO-WT). After 48 h treatment, there

was a dose-dependent and substantial increase of apoptosis in both the GDC-0449- and HH-13 treated cells as shown by Annexin V/PI staining (Fig. 4c) and PARP cleavage (Fig. 4d). Taken together, these results highlight a molecular suppression of mTOR network and induction of apoptotic death in SMO-targeted antitumor effects.

Blockade of the Hh paracrine signaling in tumor environment Paracrine signaling has an important role in Hh/SMO pathway activation of various cancers. A schematic diagram shows the in vivo paracrine stimulation of stromal Hh pathway (Fig. 5a) [25, 26]. The

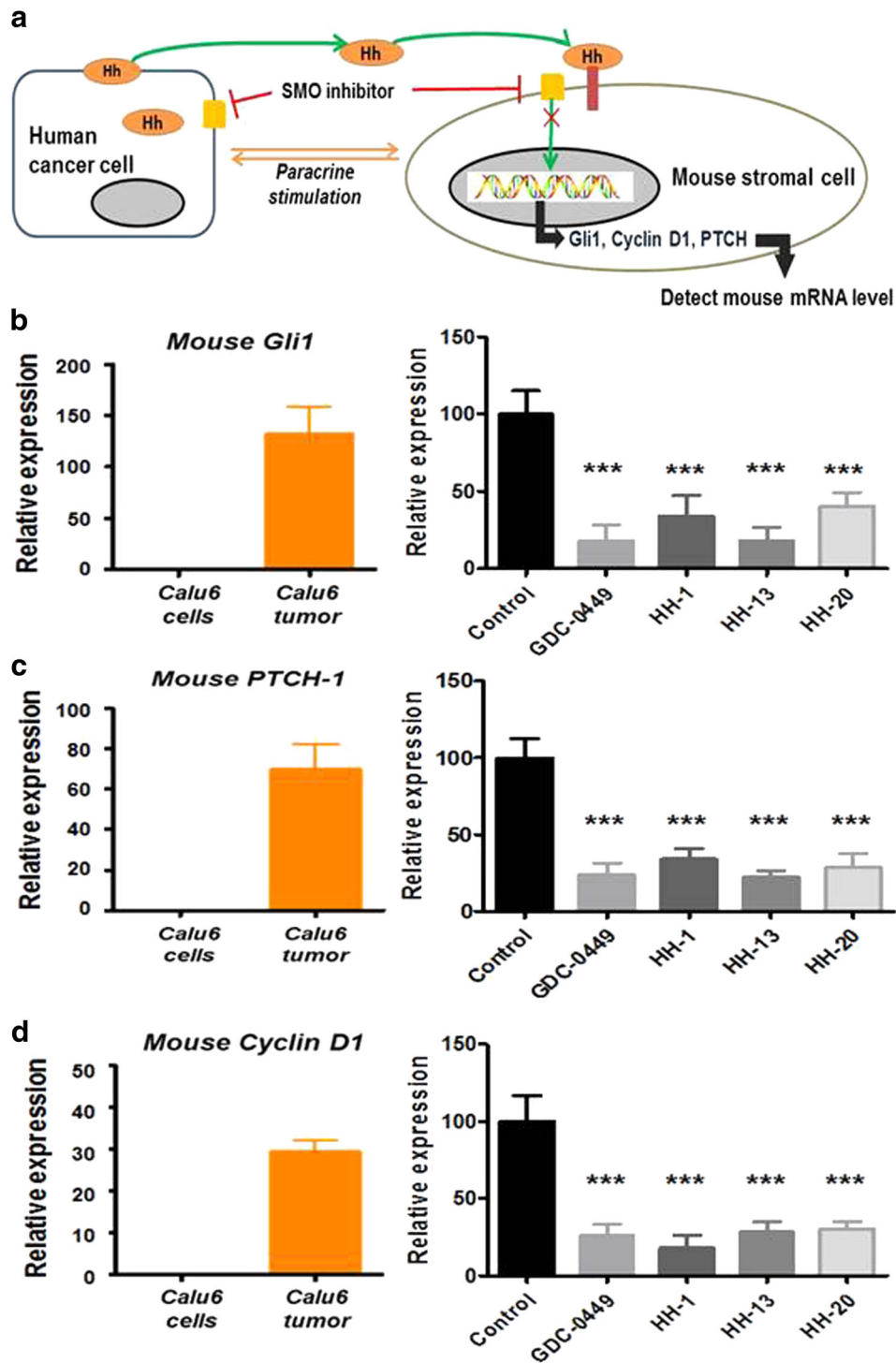


Fig. 5 New SMO inhibitors target paracrine Hh pathway in vivo. **a** Schematic diagram shows the in vivo paracrine stimulation of stromal Hh pathway. **b–d** Nude mice bearing Calu-6 tumors (~400 mm³) were dosed orally with 75 mg/kg GDC-0449, HH-1, HH-13, or HH-20 twice daily (bid) for a total of five doses. Tumors were collected and analyzed for stromal expression of mouse Hh pathway biomarkers using mouse-specific PCR primers. Tumors were analyzed for mRNA levels of mouse *Gli1* (**b**), mouse *PTCH-1* (**c**) and mouse *cyclin D1* (**d**). In RT-PCR measurements of each gene set, RNA samples of Calu-6 cells grown in cell culture dish served as a background control for the assay (left panels). For tumor results, relative expression levels are shown (right panels). Statistical analysis (treated vs. vehicle control): *** $P < 0.001$

Calu-6 lung tumor in vivo mouse model could be used as an Hh paracrine stimulation model [27]. We observed that while no mouse-specific gene expression was detected in cultured Calu-6 cells, the in vivo tumors were associated with an extensive recruitment and activation of mouse stromal *Gli1*, *PTCH-1*, and *cyclin D1* gene expression (Fig. 5b–d, left panels). Oral treatment of the Calu-6

tumor-bearing mice with HH-1, HH-13, and HH-20 (75 mg/kg, bid; total five doses) each led to a highly substantial suppression of the mouse stromal *Gli1*, *PTCH-1*, and *cyclin D1* ($P < 0.001$), which were comparable to that by GDC-0449 (Fig. 5b–d, right panels). These results indicate that similar to GDC-0449, the current series of inhibitors can effectively inhibit Hh paracrine activation in vivo.

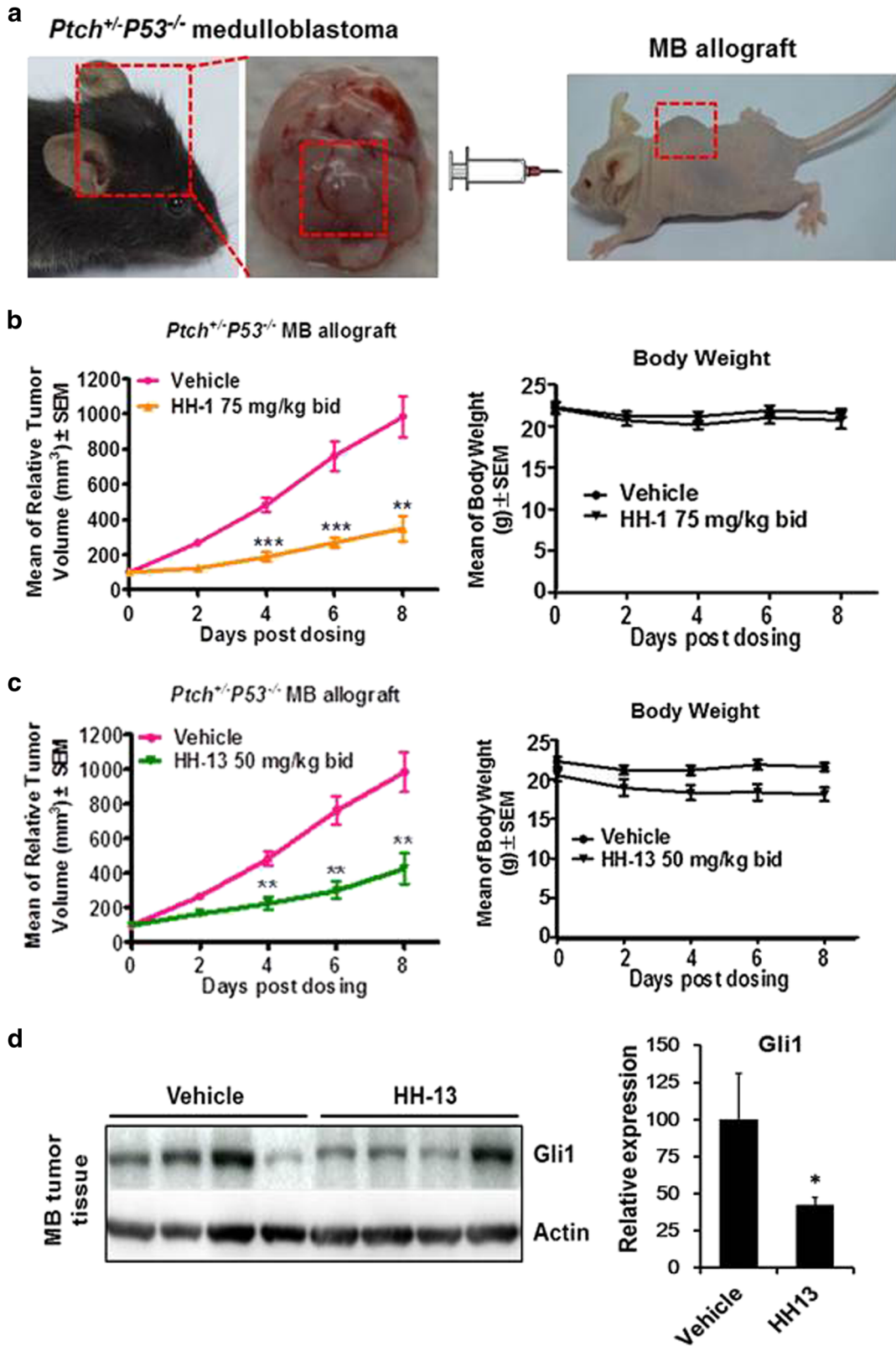


Fig. 6 Inhibition of *PTCH*^{+/-}/*P53*^{-/-} medulloblastoma (MB) allograft tumor growth in vivo. **a** Mice bearing *PTCH*^{+/-} *P53*^{-/-} MB brain tumors (left panel) and allograft tumors (right panel) are shown. **b, c** Mice bearing the staged allograft MB tumors were treated with vehicle, 75 mg/kg HH-1 (**b**) or 50 mg/kg HH-13 (**c**) following a twice daily (bid) oral dosing regimen. Tumor growth curves (left panels) and body weight changes (right panels) are shown. **d** At the end of study in **c**, tumors were collected and subjected to immunoblotting (left panel). The quantified results ($n = 4$) are plotted (right panel). Statistical analysis (treated vs. vehicle control): * $P < 0.05$; ** $P < 0.01$; *** $P < 0.001$

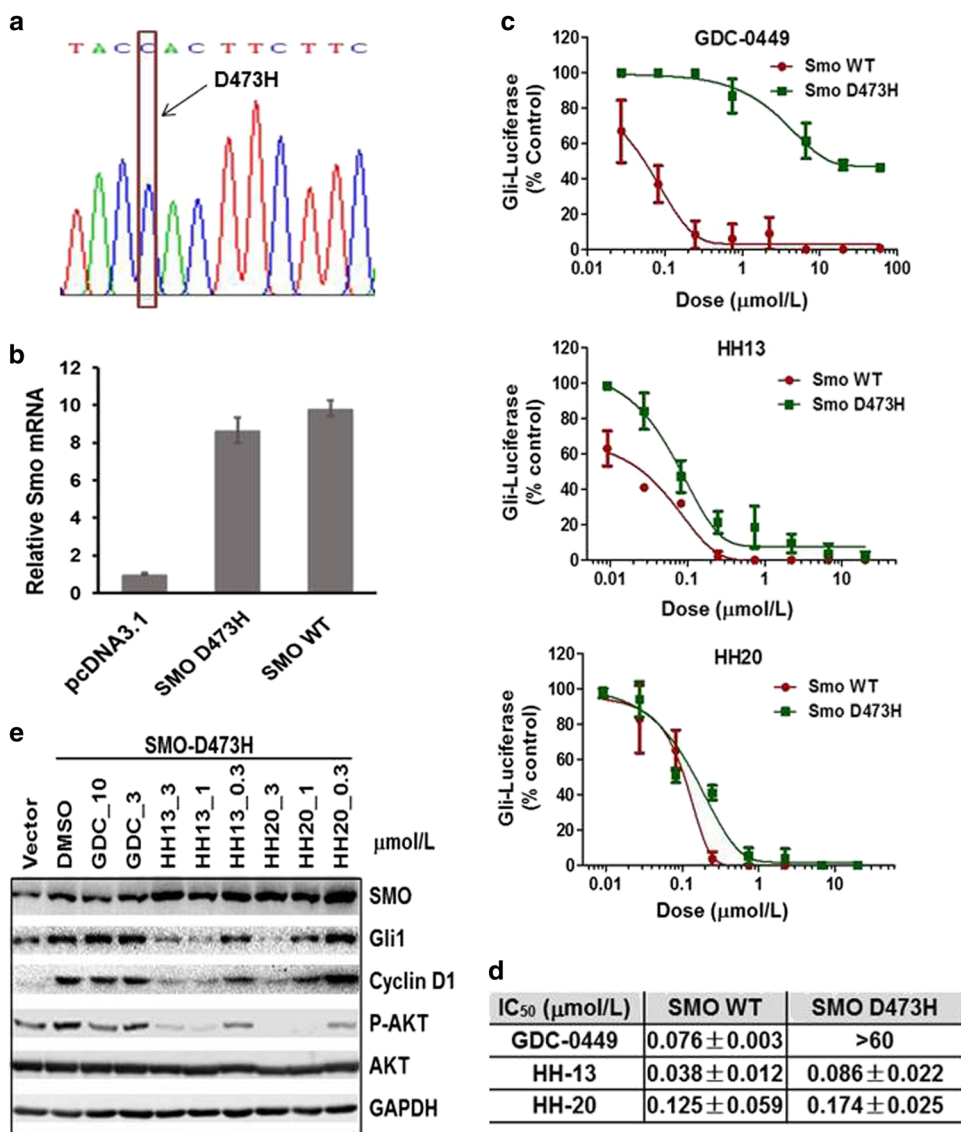


Fig. 7 HH-13 and HH-20 are effective in targeting GDC-0449-resistant SMO-D473H. **a** Construction of SMO-WT and SMO-D473H expression vectors. DNA sequence with the D473H point mutation is shown. **b** 293T cells were transfected with SMO-WT or SMO-D473H plasmids for 8 h, collected for analysis of SMO overexpression by PCR. **c, d** 293T cells were transiently transfected with Gli1-luc plus SMO-WT or Gli1-luc plus SMO-D473H plasmids for 24 h, treated with the indicated inhibitors for 48 h. Luciferase assays were performed as described in Methods. For inhibition results, dose–response curves (**c**) and IC₅₀ values (**d**) are shown. **e** 293T cells expressing the SMO-D473H were treated with inhibitors for 48 h. Cells were collected and subjected to immunoblotting

Antitumor activity in PTCH^{+/-}/P53^{-/-} medulloblastoma mouse model

There is strong evidence that nearly one third of medulloblastoma (MB) is related to the dysregulation of the Hh pathway [28] and the PTCH^{+/-}/P53^{-/-} spontaneous MB is a good experimental mouse model. [29] We established this model (Fig. 6a) and validated it using GDC-0449, which demonstrated the expected efficacy (not shown). Oral treatment of mice bearing the MB allograft tumors with 75 mg/kg HH-1 or 50 mg/kg HH-13 resulted in a significant tumor growth delay ($P < 0.01$) without overt toxicity or loss of body weight (Fig. 6b, c). Similar treatment with 50 mg/kg HH-20 showed a hint of efficacy ($P < 0.05$) (Figure S1B). The weaker in vivo activity of HH-20 may in part reflect the lower bioavailability of this compound (Figure S1A). Immunoblotting analysis showed a trend for reduced Gli1 protein in inhibitor-treated tumors compared to vehicle control ($P < 0.05$) (Fig. 6d). These results overall indicate that HH-1, HH-13, and HH-20 can

elicit in vivo targeting of Hh-signaling function and the pathway-driven tumor growth, albeit less potent than required for drug development.

HH-13 and HH-20 potentially target GDC-0449-resistant Smoothened D473H mutation

Finally, to investigate whether the current inhibitor series could overcome acquired drug resistance to the first generation SMO inhibitors, we established the smoothened D473H mutant expression construct [16] (Fig. 7a). Upon transfection into 293T cells, both the SMO wide-type (SMO-WT) and SMO-D473H mutant (SMO-D473H) could be expressed with similar yields (Fig. 7b). In parallel Gli1-luc reporter assays of SMO-WT and SMO-D473H, GDC-0449 potently inhibited the activation of SMO-WT (IC₅₀: 0.076 $\mu\text{mol/L}$) but was poorly active in the assay for SMO-D473H (IC₅₀: >60 $\mu\text{mol/L}$) (Fig. 7c, top panel). In contrast, both HH-13 and HH-20 retained decent inhibition potency when

assayed against SMO-D473H, achieving IC₅₀ values of 0.086 and 0.174 μmol/L, respectively (Fig. 7c, d). To further confirm these results, we examined the effect on down-regulating the signaling biomarker driven by SMO-D473H. In 293T cells transfected with SMO-D473H, there was a coordinated activation in Gli1, cyclin D1, and P-AKT (Fig. 7e). Although these SMO-D473H-dependent signaling biomarkers were largely resistant to GDC-0449, they were dose dependently blocked by HH-13 and HH-20 with approximate EC₅₀ values of 0.3 μmol/L and 1 μmol/L, respectively (Fig. 7e). Thus, these results overall indicate that both HH-13 and HH-20 could effectively target the GDC-0449-resistant SMO-D473H mutation.

DISCUSSION

The FDA-approved Vismodegib/GDC-0449 and Sonidegib/LDE225 have presented a new hope for surgery unfavorable metastatic BCC patients [30, 31]. Other SMO inhibitors under development also showed positive responses in disease control [32, 33]. These achievements have spurred a new wave of SMO inhibitor research. As part of expanded discovery efforts, we uncovered a new series of SMO inhibitors, exemplified by HH-1, HH-13, and HH-20 that potently target the Hh/SMO/Gli1 pathway function in vitro and in vivo. Strong evidence points to the aberrant Hh signaling as cancer driver in advanced BCC and PTCH-deficient MB molecular type [5, 34]. The current inhibitor series are shown to inhibit the Hh pathway-driven cell proliferation accompanying G₀/G₁ cell cycle blockade and reduction of the pathway target gene expression. Moreover, in the Hh-driven PTCH^{+/-} MB in vivo model, both HH-1 and HH-13 attenuated allograft tumor growth, which correlated with the downregulation of pathway related gene expression.

As SMO inhibitors display profound anti-proliferation capacity in the Hh-driven NIH3T3 model and MB allografts, some studies observed no direct correlation between downregulation of pathway genes and in vitro anti-proliferative response in certain cancer cells [35]. Emerging evidence now supports a role for paracrine Hh signaling activation in tumorigenesis [35, 36]. Indeed, our work confirmed the presence of lung tumor cell Hh-induced paracrine stromal activation in mice, in which the tumor-induced stromal expression of Gli1, PTCH-1, and cyclin D1 were all blocked by orally administered GDC-0449 and current series of SMO inhibitors.

Downregulation of mTOR/AKT signaling function has an important role in SMO inhibitor-mediated growth suppression. The relationship was also observed in ovarian cancer cells in which depletion of AKT gene could partially reverse Gli1-induced EMT [37]. In chronic lymphocytic leukemia cell line, a Gli1 inhibitor GAN61 inhibited AKT phosphorylation [38]. In our studies, both GDC-0449 and current series of inhibitors reduced P-TSC2 (T1462) resulting in higher suppressive activity toward mTORC1. Likewise, both inhibitor classes targeted mTORC2 substrate P-AKT (S473) and its secondary readout MCL-1 [24]. Because MCL-1 is a well-characterized inhibitor of apoptosis, suppression of MCL-1 in this setting likely contributed to the efficacy of SMO inhibitors. Although the exact mechanism on how Hh/SMO signals to TSC2/mTORC1 or mTORC2/AKT remains to be elucidated, the results of current work and previous reports highlight a critical role for mTOR network in the Hh pathway-dependent cancer cell growth and tumorigenesis [38–41].

Acquired drug resistance and tumor relapse are weaknesses of the first generation SMO-targeted drugs. Our inhibitors are intended to overcome the clinically prevalent smoothened mutation SMO-D473H, which renders GDC-0449 and LDE225 binding inefficient and clinical resistance. We have shown that in contrast to GDC-0449, both HH-13 and HH-20 elicited potent inhibition of SMO-D473H. This conclusion is based on their activity in specific suppression of SMO-D473H-driven Gli1-reporter signal

and the blockade of SMO-D473H-driven cellular pathway biomarkers. Additional support for specific SMO-targeting by these compounds came from their structure and activity relationship (SAR) profile. In this SAR process, when we varied substituent on the pyridine ring and amide benzene ring, their activity behaviors were very similar to the SAR profile for GDC-0449 [42]. A major deficiency of our study is the lack of direct binding data on these inhibitors to purified SMO proteins. Future studies are required to elucidate the inhibitor binding mode to both the naïve and drug-resistant SMO variants. Collectively, the current inhibitors may present an opportunity for medicinal chemistry optimization on pharmaceutical property towards the development of new generation SMO inhibitor therapy.

ACKNOWLEDGEMENTS

This work was supported by a startup grant from Fudan University (EZF301002) and National Natural Science Foundation of China (81273367). We thank Fudan University School of Pharmacy Animal Facility and Instrument Center for excellent technical support.

AUTHOR CONTRIBUTIONS

Conception and design: H.L., K.Y. Development of methodology: H.Z., Q.L., K.Y. Acquisition of data: H.Z., Q.L., X.Z. Analysis and interpretation of data: H.Z., Q.L., X.Z. Writing, review, and/or revision of the manuscript: Q.L., H.L., K.Y. Administrative, technical, or material support: H.L., K.Y. Study supervision: K.Y.

ADDITIONAL INFORMATION

The online version of this article (<https://doi.org/10.1038/s41401-018-0019-5>) contains supplementary material, which is available to authorized users.

Competing interests: The authors declare no competing interests.

REFERENCES

- Ishibashi M, McMahon AP. A sonic hedgehog-dependent signaling relay regulates growth of diencephalic and mesencephalic primordia in the early mouse embryo. *Development*. 2002;129:4807–19.
- Pasca DMM, Hebrok M. Hedgehog signalling in cancer formation and maintenance. *Nat Rev Cancer*. 2003;3:903–11.
- Amakye D, Jagani Z, Dorsch M. Unraveling the therapeutic potential of the Hedgehog pathway in cancer. *Nat Med*. 2013;19:1410–22.
- Yang L, Xie GQ, Xie J. Activation of the hedgehog-signaling pathway in human cancer and the clinical implications. *Oncogene*. 2010;29:469–81.
- Teglund S, Toftgard R. Hedgehog beyond medulloblastoma and basal-cell carcinoma. *Biochim Et Biophys Acta*. 2010;1805:181–208.
- Harris LG, Samant RS, Shevde LA. Hedgehog signaling: networking to nurture a pro-malignant tumor microenvironment. *Mol Cancer Res*. 2011;9:1165–74.
- Ehteshami M, Sarangi A, Valadez JG, Chanthaphaychith S, Becher MW, Abel TW, et al. Ligand-dependent activation of the hedgehog pathway in glioma progenitor cells. *Oncogene*. 2007;26:5752–61.
- Athar M, Li C, Tang X, Chi S, Zhang X, Kim AL, et al. Inhibition of smoothened signaling prevents ultraviolet B-induced basal cell carcinomas through regulation of Fas expression and apoptosis. *Cancer Res*. 2004;64:7545–52.
- Dummer R, Guminski A, Gutzmer R, Dirix L, Lewis KD, Combemale P, et al. The 12-month analysis from basal cell carcinoma outcomes with LDE225 treatment (BOLT): a phase II, randomized, double-blind study of sonidegib in patients with advanced basal cell carcinoma. *J Am Acad Dermatol*. 2016;75:113–25.
- Von Hoff DD, Lorusso PM, Rudin CM, Reddy JC, Yauch RL, Tibes R, et al. Inhibition of the hedgehog pathway in advanced basal-cell carcinoma. *New Engl J Med*. 2009;361:1164–72.
- Watkins DN, Berman DM, Burkholder SG, Wang B, Beachy PA, Baylin SB. Hedgehog signalling within airway epithelial progenitors and in small-cell lung cancer. *Nature*. 2003;422:313–7.
- Yauch RL, Dijkgraaf GJP, Aliche B, Januario T, Ahn CP, Holcomb T, et al. Smoothened mutation confers resistance to a hedgehog pathway inhibitor in medulloblastoma. *Science*. 2009;326:572–4.
- Sharpe HJ, Pau G, Dijkgraaf GJ, Bassetseguin N, Modrusan Z, Januario T, et al. Genomic analysis of smoothened inhibitor resistance in basal cell carcinoma. *Cancer Cell*. 2015;27:327–41.

14. Danial C, Sarin KY, Oro AE, Chang AL. An investigator-initiated open-label trial of sonidegib in advanced basal cell carcinoma patients resistant to vismodegib. *Clin Cancer Res.* 2016;22:1325–9.
15. Sharpe HJ, Pau G, Dijkgraaf GJ, et al. Genomic analysis of smoothened inhibitor resistance in basal cell carcinoma. *J Cancer Cell.* 2015;27:327–41.
16. Atwood SX, Sarin KY, Whitson RJ, Li JR, Kim G, Rezaee M, et al. Smoothened variants explain the majority of drug resistance in basal cell carcinoma. *J Cancer Cell.* 2015;27:342–53.
17. Ishii T, Shimizu Y, Nakashima K, Kondo S, Ogawa K, Sasaki S, et al. Inhibition mechanism exploration of investigational drug tak-441 as inhibitor against vismodegib-resistant smoothened mutant. *Eur J Pharmacol.* 2014;723:305–13.
18. Peukert S, He F, Dai M, Zhang R, Sun Y, Miller-Moslin K, et al. Cover picture: discovery of nvp-leq506, a second-generation inhibitor of smoothened (chem-medchem 8/2013). *ChemMedChem.* 2013;8:1261.
19. Lee MJ, Hatton BA, Villavicencio EH, Khanna PC, Friedman SD, Ditzler S, et al. Hedgehog pathway inhibitor saridegib (ipi-926) increases lifespan in a mouse medulloblastoma model. *Proc Natl Acad Sci USA.* 2012;109:7859–64.
20. Lang, H., Yu, K., & Zhao, H. Benzimidazole compound with antitumour activity as well as preparation method and application thereof. Patent Application CN201310139335.
21. Lang, H., Yu, K., & Zhao, H. Benzimidazole amide compound as well as preparation method and application thereof. Patent Application CN201310186206.
22. Koo J, Yue P, Deng X, Khuri FR, Sun SY. mTOR complex 2 stabilizes Mcl-1 protein by suppressing its glycogen synthase kinase 3-dependent and SCF-FBXW7-mediated degradation. *Mol Cell Biol.* 2015;35:2344–55.
23. Li X, Wang Z, Ma Q, Xu Q, Liu H, Duan W, et al. Sonic hedgehog paracrine signaling activates stromal cells to promote perineural invasion in pancreatic cancer. *Clin Cancer Res.* 2014;20:4326–38.
24. Lubik AA, Nouri M, Truong S, Ghaffari M, Adomat HH, Corey E, et al. Paracrine sonic hedgehog signaling contributes significantly to acquired steroidogenesis in the prostate tumor microenvironment. *Int J Cancer.* 2017;140:358–69.
25. Robarge KD, Brunton SA, Castaneda GM, Cui Y, Dina MS, Goldsmith R, et al. GDC-0449—a potent inhibitor of the hedgehog pathway. *Bioorg Med Chem Lett.* 2009;19:5576–81.
26. Kool M, Korshunov A, Remke M, Jones DT, Schlanstein M, Northcott PA, et al. Molecular subgroups of medulloblastoma: an international metaanalysis of transcriptome, genetic aberrations, and clinical data of WNT, SHH, Group 3, and group 4 medulloblastomas. *Acta Neuropathol.* 2012;123:473–84.
27. Romer JT, Kimura H, Magdaleno S, Sasai K, Fuller C, Baines H, et al. Suppression of the Shh pathway using a small molecule inhibitor eliminates medulloblastoma in Ptc1(+/-)p53(-/-) mice. *Cancer Cell.* 2004;6:229–40.
28. Dummer R, Guminski A, Gutzmer R, Dirix L, Lewis K, Combemale P, et al. LBA33 randomized, double-blind study of sonidegib (LDE225) in patients (PTS) with advanced basal cell carcinoma (BCC). *Ann Oncol.* 2014;25:1–41.
29. Chang ALS, Solomon JA, Hainsworth JD, Goldberg L, McKenna E, Day B-M, et al. Expanded access study of patients with advanced basal cell carcinoma treated with the hedgehog pathway inhibitor, vismodegib. *J Am Acad Dermatol.* 2014;70:60–9.
30. Sasaki K, Gotlib JR, Mesa RA, Newberry KJ, Ravandi F, Cortes JE, et al. Phase II evaluation of IPI-926, an oral hedgehog inhibitor, in patients with myelofibrosis. *Leuk Lymphoma.* 2015;56:2092–7.
31. Wagner AJ, Messersmith WA, Shaik MN, Li S, Zheng X, McLachlan KR, Cesari R, Courtney R, Levin WJ, El-Khoueiry AB. A phase I study of PF-04449913, an oral hedgehog inhibitor, in patients with advanced solid tumors. *Clin Cancer Res.* 2015;21:1044–51.
32. Remke M, Hielscher T, Northcott PA, Witt H, Ryzhova M, Wittmann A, et al. Adult medulloblastoma comprises three major molecular variants. *J Clin Oncol.* 2011;29:2717–23.
33. Yauch RL, Gould SE, Scales SJ, Tang T, Tian H, Ahn CP, et al. A paracrine requirement for hedgehog signalling in cancer. *Nature.* 2008;455:406–10.
34. Ingram WJ, Wicking CA, Grimmond SM, Forrest AR, Wainwright BJ. Novel genes regulated by sonic hedgehog in pluripotent mesenchymal cells. *Oncogene.* 2002;21:8194–205.
35. Ke Z, Caiping S, Qing Z, Xiaojing W. Sonic hedgehog-Gli1 signals promote epithelial-mesenchymal transition in ovarian cancer by mediating PI3K/AKT pathway. *Med Oncol.* 2015;32:368.
36. Kern D, Regl G, Hofbauer SW, Altenhofer P, Achatz G, Dlugosz A, et al. Hedgehog/GLI and PI3K signaling in the initiation and maintenance of chronic lymphocytic leukemia. *Oncogene.* 2015;34:5341–51.
37. Buonamici S, Williams J, Morrissey M, Wang A, Guo R, Vattay A, et al. Interfering with resistance to smoothened antagonists by inhibition of the PI3K pathway in medulloblastoma. *Sci Transl Med.* 2010;2:51ra70.
38. Metcalfe C, Alicke B, Crow A, Lamoureux M, Dijkgraaf GJ, Peale F, et al. PTEN loss mitigates the response of medulloblastoma to hedgehog pathway inhibition. *Cancer Res.* 2013;73:7034–42.
39. Sharma N, Nanta R, Sharma J, Gunewardena S, Singh KP, Shankar S, et al. PI3K/AKT/mTOR and sonic hedgehog pathways cooperate together to inhibit human pancreatic cancer stem cell characteristics and tumor growth. *Oncotarget.* 2015;6:32039–60.
40. Dijkgraaf GJ, Alicke B, Weinmann L, Januario T, West K, Modrusan Z, et al. Small molecule inhibition of GDC-0449 refractory smoothened mutants and downstream mechanisms of drug resistance. *Cancer Res.* 2011;71:435–44.
41. Yu K, Toral-barza L, Shi C, Zhang WG, Lucas J, Shor B, et al. Biochemical, cellular, and in vivo activity of novel ATP-competitive and selective inhibitors of the mammalian target of rapamycin. *Cancer Res.* 2009;69:6232–40.
42. Wetmore C, Eberhart DE, Curran T. Loss of p53 but not ARF accelerates medulloblastoma in mice heterozygous for patched. *Cancer Res.* 2001;61:513–6.